Supporting Information

for

Phenazines-Integrated Conjugated Microporous Polymers for Modulating the Mechanics of Supercapacitor Electrodes

Mohammed G. Kotp,[a] Johann Lüder,[a,b] Shiao-Wei Kuo,[a] and Ahmed F. M. EL-Mahdy*[a,c]

a. Department of Materials and Optoelectronic Science, National Sun Yat-Sen University, Kaohsiung, 80424, Taiwan
b. Center for Theoretical and Computational Physics, National Sun Yat-Sen University, Kaohsiung 80424, Taiwan
c. Chemistry Department, Faculty of Science, Assiut University, Assiut 71516, Egypt.

Corresponding Author:

E-mail: ahmedelmahdy@mail.nsysu.edu.tw (A. F. M. EL-Mahdy)

S.1 Materials

NO.	MATERIAL	SUPPLIER
1	1,1′Bis(diphenylphosphino)ferrocene]dichloropalladium(II)Pd(dppf)Cl_2	San Diego, USA
2	Palladium-tetrakis(triphenylphosphine) ($Pd(PPh_3)_4$)	Sigma Aldrich, USA
3	potassium carbonate (K_2CO_3)	Sigma Aldrich, USA
4	N-Bromo-succinimide (NBS)	TCI, USA
5	Ammonium hydroxide (NH_4OH)	TCI, USA
6	Tin (II) chloride ($SnCl_2$)	TCI, USA
7	Potassium hydroxide (KOH)	TCI, USA
8	Dioxane	TCI, USA
9	DMF	TCI, USA
10	EtOH	TCI, USA
11	Acetic acid	TCI, USA
12	Triethylamine	Sigma Aldrich, USA

S.2 Characterizations

FTIR tests were achieved through synthesis of classical KBr disks then scanned by a Bruker Tensor 27 FTIR spectrophotometer in the wavenumber range between 550:4000 cm^{-1} and 4 cm^{-1} resolution rate. Both ^1H and ^{13}C NMR scans examined after solvation our monomers in $CDCl_3$ by an INOVA 500 instrument and applying Tetramethylsilane (TMS) as an out reference, moreover, chemical shifts were recorded by part per million (ppm). Thermo gravimetric analysis (TGA) of our polymers were achieved under nitrogen environment through well closing of them in Pt cell then raising the temperature to 800 °C by regular raising rate 20 °C min^{-1}. Solid state nuclear magnetic resonance (SSNMR) profiles were achieved via Bruker Avance 400 NMR instrument which has Buruker magic-angle-spinning (MAS) sensor (32,000 scans). Surface areas and porosities measurements of our synthesized polymers were achieved through Micromeritics ASAP 2020 surface area and porosity analyser, measurements occurred after complete degassing of our samples. Gaining nitrogen isotherms was supported more by the progressive exposure to high purity N_2 in liquefied nitrogen. A JEOL JSM-7610F scanning electron microscope was used for surface visualization (FE-SEM), furthermore, prior to visualization samples films were coated by Pt (Pt sputtering) for 150 s for superior monitoring. Transmission electron microscopy (TEM) images were formed via using the modified JEOL-2100 scanning electron microscope at 200 KV.

S.3 Synthetic Methodologies

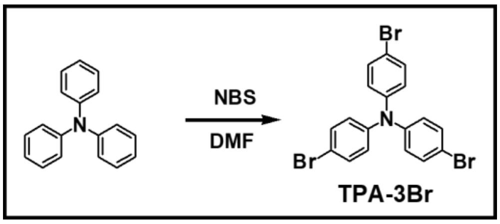

Scheme S1 Synthesis of Tris(4-bromophenyle)amine (TPA-3Br).

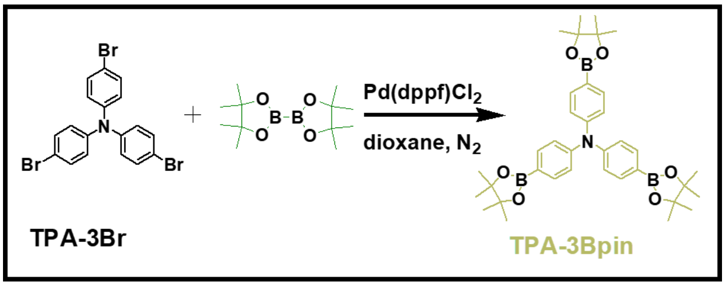

Scheme S2 Synthesis of tris(4-(4,4,5,5-tetramethyl-1,3,2-dioxaborolan-2-yl)phenyl)amine (TPA-3Bpin).

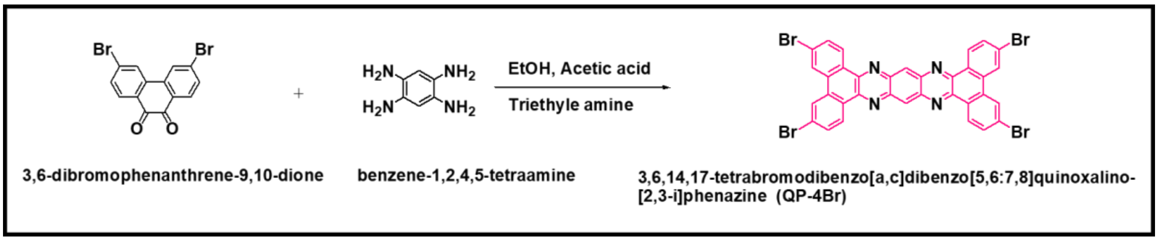

Scheme S3 Synthesis of 3,6,14,17-tetrabromodibenzo[a,c]- dibenzo[5,6:7,8]-quinoxalino-[2,3-i]phenazine (QP-4Br).

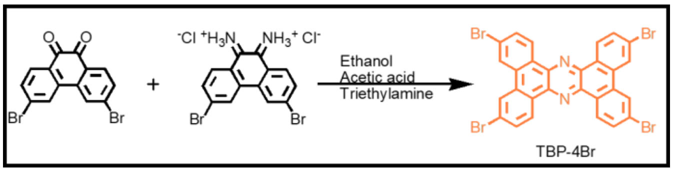

Scheme S4 Synthesis of tetrabromotetrabenzophenazine (TBP-4Br).

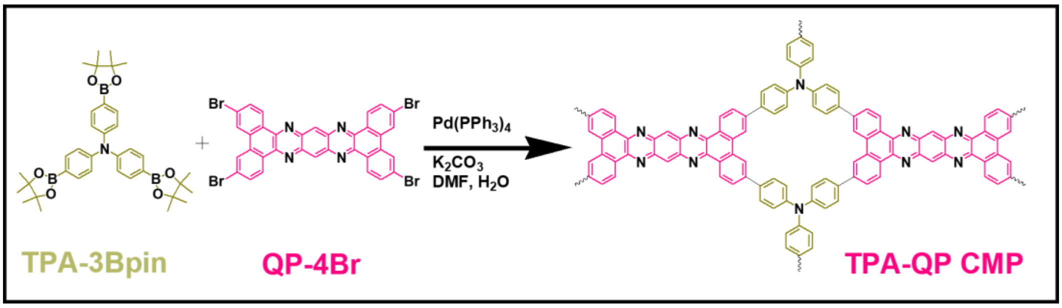

Scheme S5 Synthesis of TPA-QP CMP.

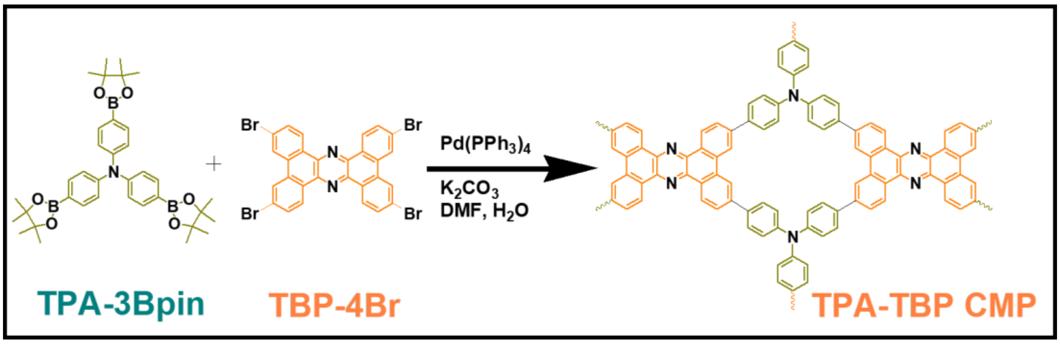

Scheme S6 Synthesis of TPA-TBP CMP.

__S.4 FTIR Spectral Profiles__

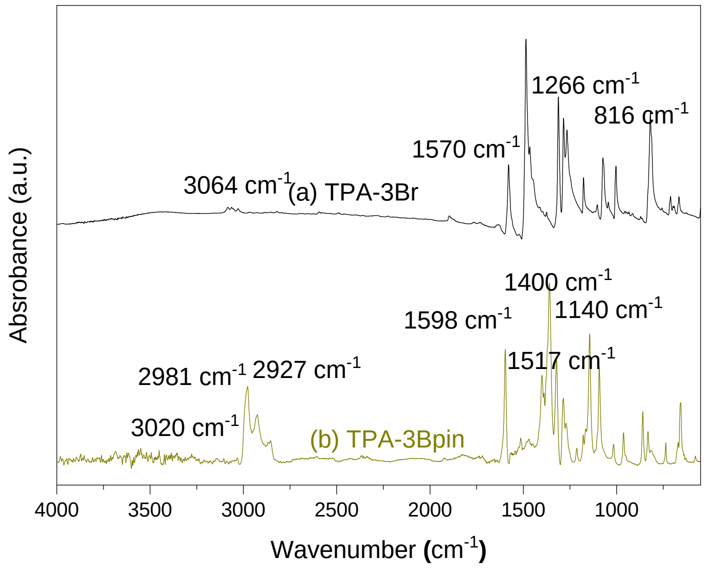

Fig. S1 FTIR spectrum of TPA-Br, and TPA-3Bpin.

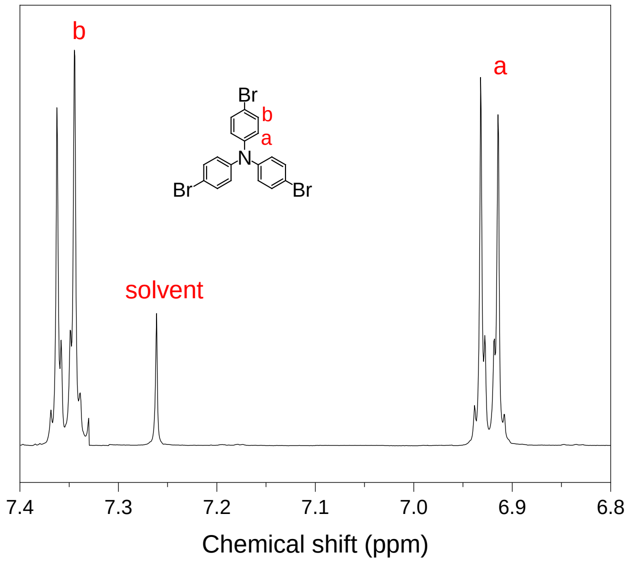

Fig. S2 ^{1}H NMR spectrum of TPA-3Br.

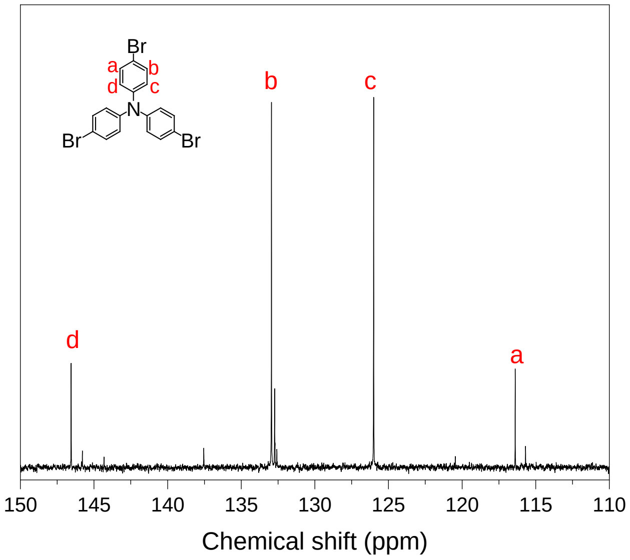

Fig. S3 ^{13}C NMR spectrum of TPA-3Br.

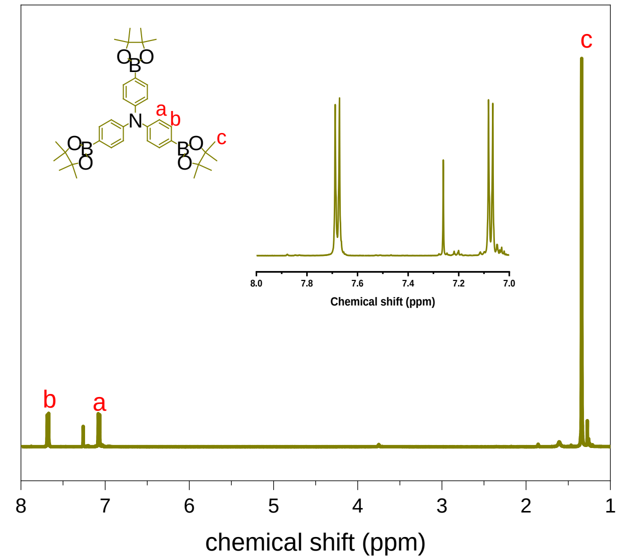

Fig. S4 ^{1}H NMR spectrum of TPA-Bpin.

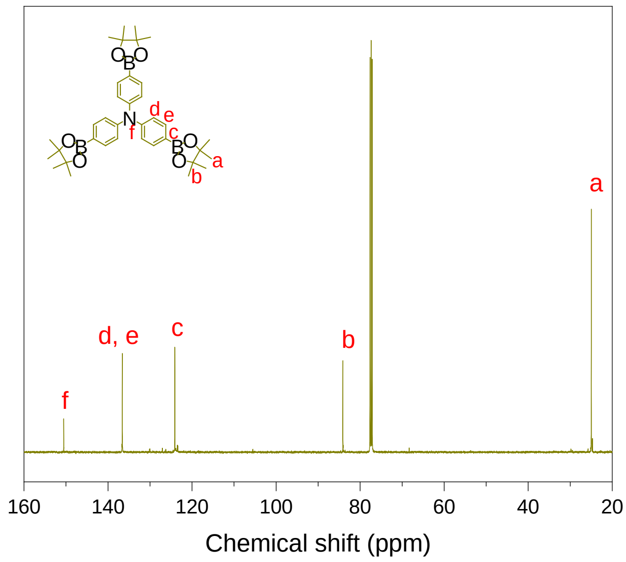

Fig. S5 ^{13}C NMR spectrum of TPA-3Bpin.

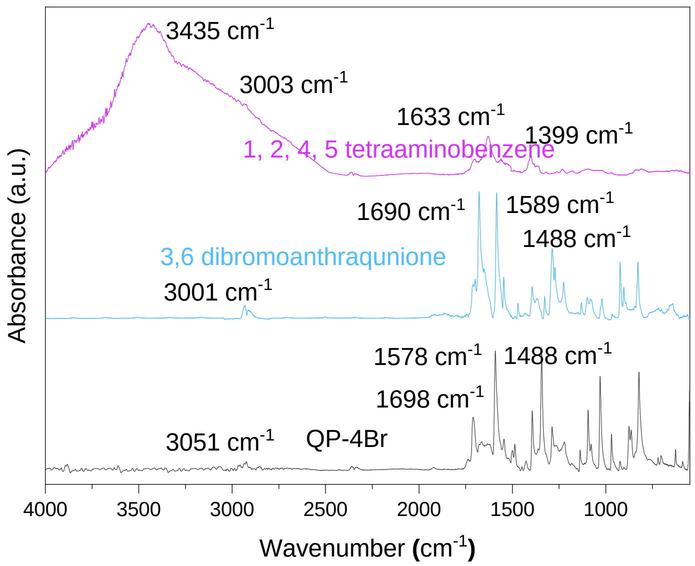

Fig. S6 FTIR spectrum of 1,2,4,5 tetramino-benzene, 3,6-dibromophenanthrene-9,10-dione, and QP-4Br.

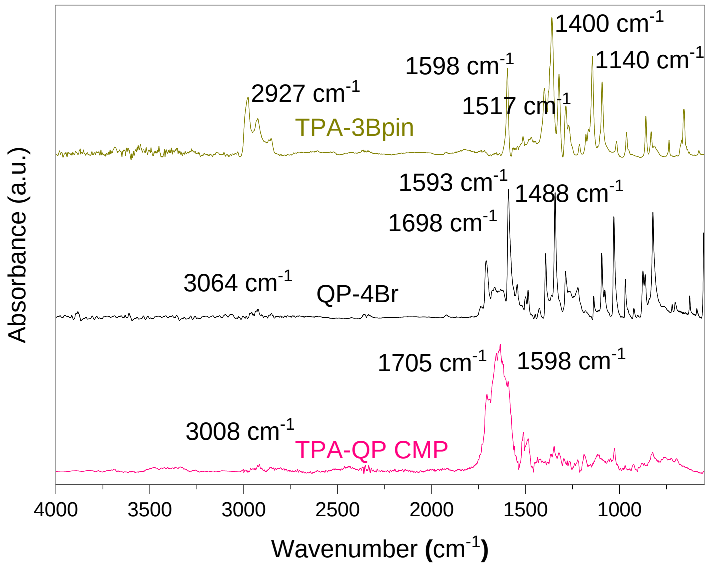

Fig. S7 FTIR spectrum of TPA-Bpin, QP-4Br, and TPA-QP CMP.

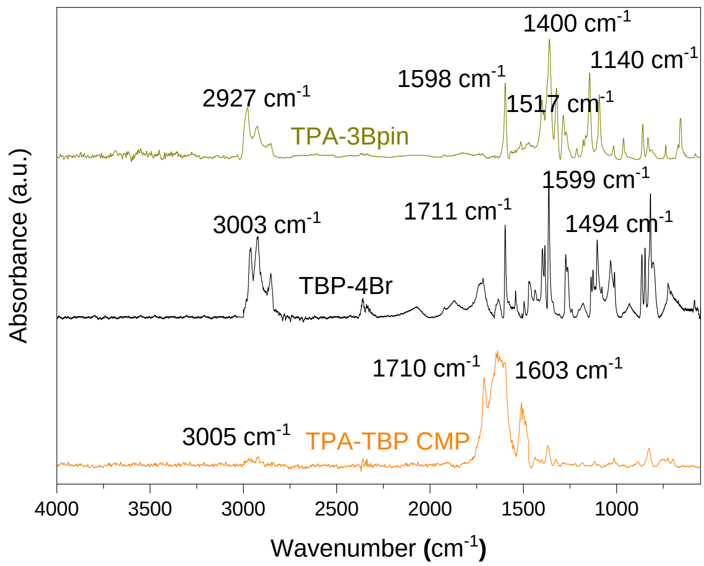

Fig. S8 FTIR spectrum of TPA-Bpin, TBP-4Br, and TPA-TBP CMP.

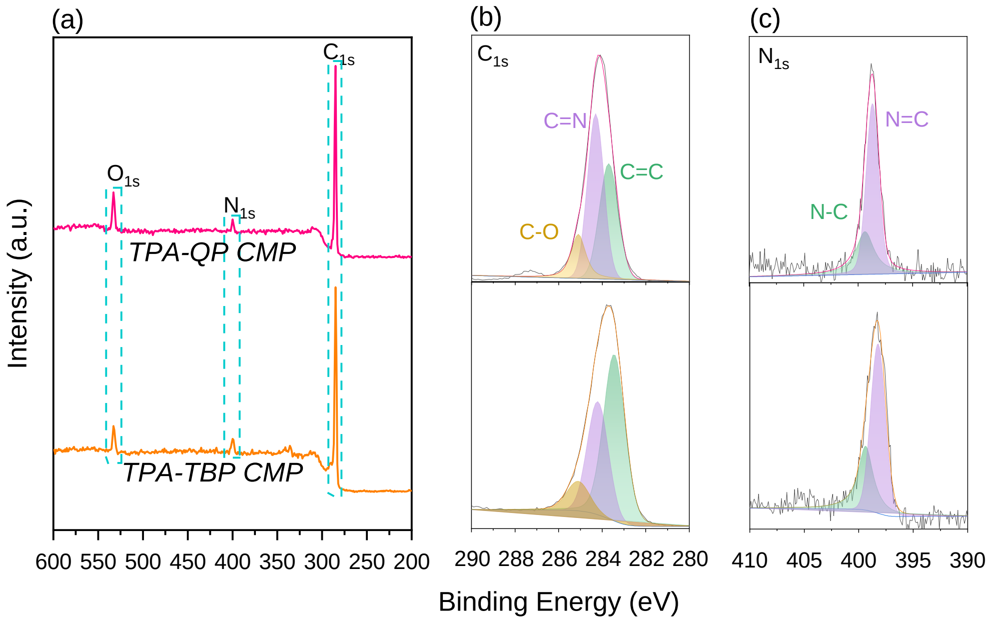

Fig.S9 Wide-scan XPS profiles (a), High-resolution XPS profiles attributed to the C 1s (b), and N 1s (c), of TPA-QP and TPA-TBP CMPs respectively.

Table S1 FWHM and area of various species detected through XPS

CMP	**C1s**						**N1s**			
	C=C (283.7 eV)		C=N (284.3 eV)		C-O (285.1 eV)		N-C (399.36 eV)		N=C (398.6 eV)	
	FWHM	Area	FWHM	Area	FWHM	Area	FWHM	Area	FWHM	Area
TPA-QP	1.02	44427.27	0.89	5536.183	0.8	1730.391	1.9828	330.7931	1.37	675.8508
TPA-TBP	1.17	7641.939	1.15	4703.811	1.24	1374.997	1.67	466.48	1.6	802.9703

S.5 Thermal gravimetric analysis

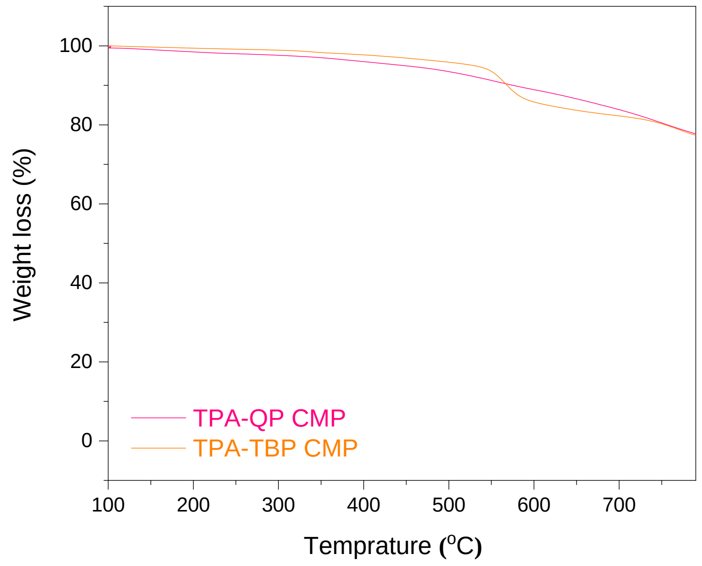

Fig.S10 TGA analyses of the TPA-QP and TPA-TBP CMPs.

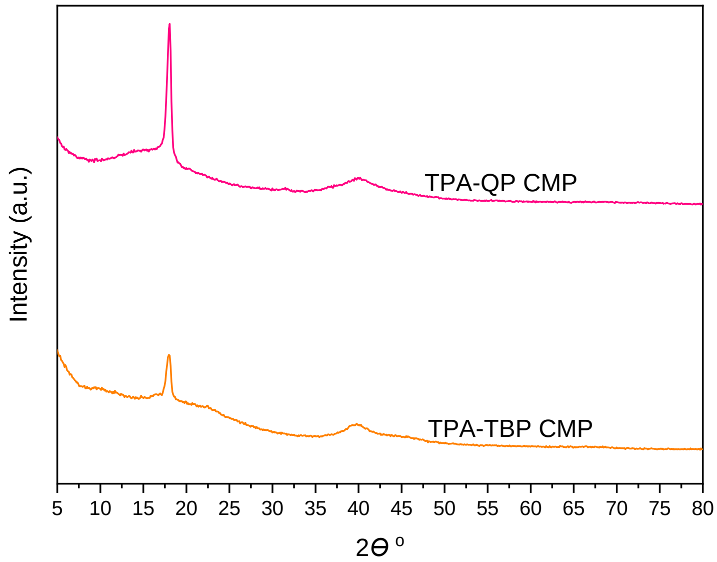

Fig. S11 XRD of TPA-QP, and TPA-TBP CMPs

S.6 Electrochemical analysis

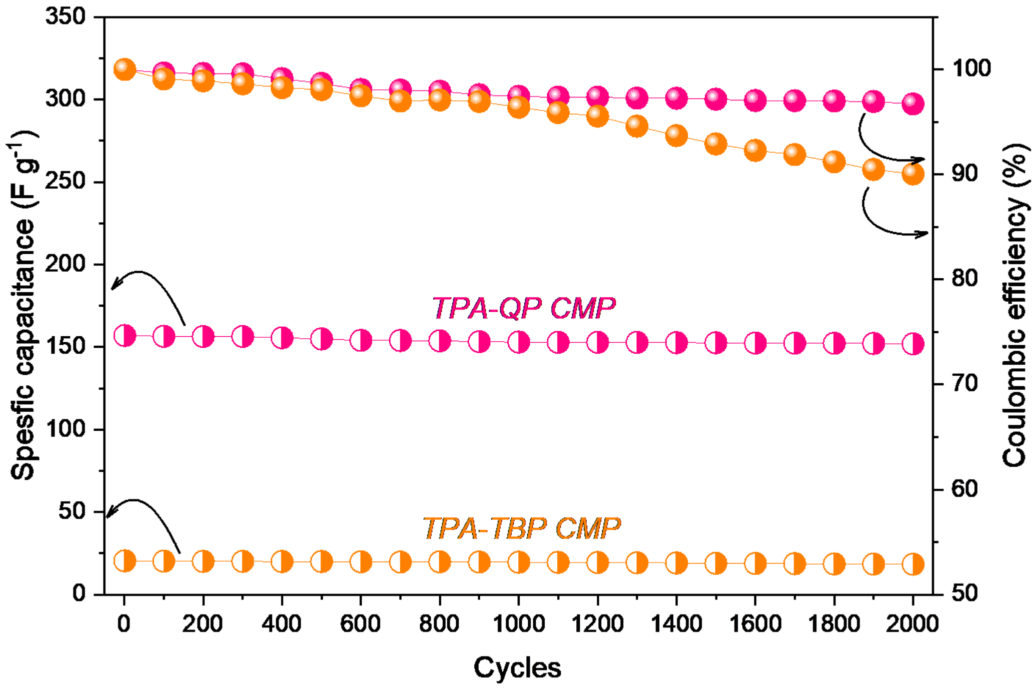

Fig. S12 Specific capacitance supported by Coulombic efficiency of TPA-QP (pink) and TPA-TBP (orange) CMPs measured at current density 10 A g^{-1} within 2000 cycles.

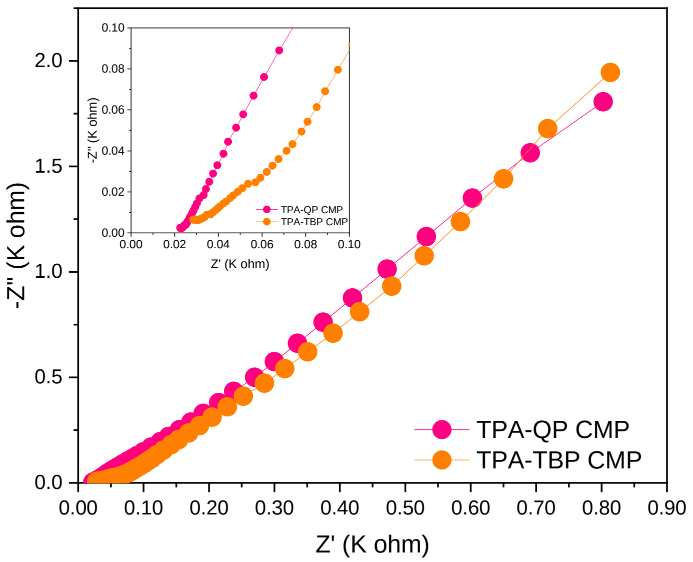

Fig. S13 EIS spectra of TPA-QP and TPA-TBP CMPs.

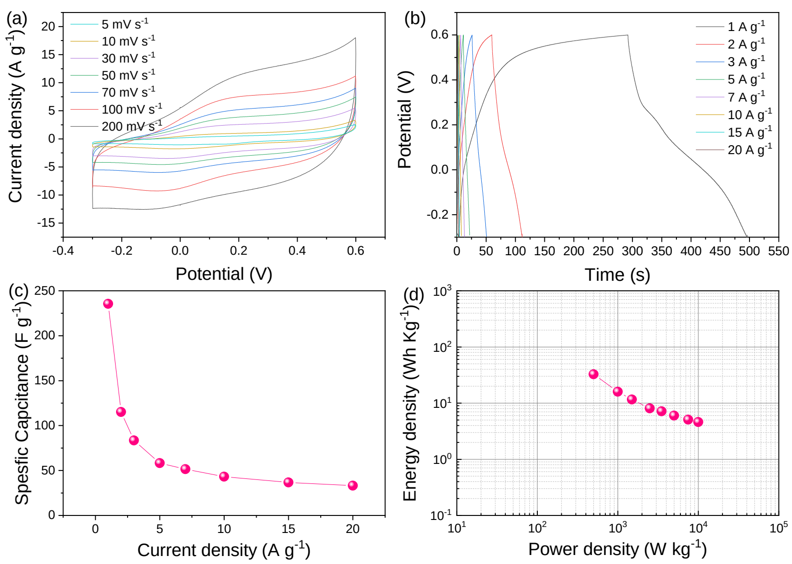

Fig. S14 CV plateaus (a), GCD curves b), specific capacitances at various current densities (c), and Ragone plot (d) of SSC coin cells incorporating TPA-QP CMP.

S.7 Comparison study

Table S2 Comparison study between energy density alongside power density of QP CMPs with previously reported electrodes

Polymer	***Energy density (W kg^{-1})***	***Power density (Wh kg^{-1})***	***Ref.***
PANI/NCNT	11.1	980	[1]
MCSF	9.6	108.5	[2]
IHPNC- carbon nanotubes	8.7	195	[3]
N-PCNFs/PSN	8.5	250	[4]
N-CNFs/900	7.11	125	[5]
FC-CMPs/rGO	8	124	[6]
TPA-QP CMP	50.417	500	This work
TPA-TBP CMP	5	500	This work

Table S3 Comparison study between specific surface areas/specific capacitances of TPA-QP and TPA-TBP CMPs with previously reported porous materials employed as supercapacitor electrodes.

Material	Surface area (m^2 g^{-1})	Capacitance (F g^{-1})	Current density (A g^{-1})	Reference
N-CMP	267	71	1	[7]
CoPc-CMP	N/A	13.7	1	[8]
DAAQ-TFP COF thin film	N/A	3	150	[9]
N-doped porous nanofibers	562	202	1	[5]
NWNU- COF-1	301	155.38	0.25	[10]
DAB-TFP COF	385	98	0.5	[11]
An-CPOP-1	580	72.75	0.5	[12]
An-CPOP-2	1130	98.4	0.5	[12]
PAQBz	N/A	106	0.3	[13]
TPA–COF–1	714	51.3	0.2	[14]
TPA–COF–2	478	14.4	0.2	[14]
TPA–COF–3	557	5.1	0.2	[14]
TPT–COF–4	1132	2.4	0.2	[14]
TPT–COF–5	1747	0.34	0.2	[14]
TPT–COF–6	1535	0.24	0.2	[14]
DAAQ–TFP COF	1280	48	0.1	[15]
TPA-QP CMP	815	356	1	This study
TPA-TBP CMP	238	88	1	This study

References and Notes

1 R. Malik, L. Zhang, C. Mcconnell, M. Schott, Y.-Y. Hsieh, R. Noga, N. T. Alvarez and V. Shanov, Carbon, 2017, **116**, 579-590.

2 Q. Wang, J. Yan, T. Wei, J. Feng, Y. Ren, Z. Fan, M. Zhang and X. Jing, Carbon, 2013, **60**, 481-487.

3 S. Zuo, J. Chen, W. Liu, X. Li, Y. Kong, C. Yao and Y. Fu, Carbon, 2018, **129**, 199-206.

4 Q. Meng, K. Qin, L. Ma, C. He, E. Liu, F. He, C. Shi, Q. Li, J. Li and N. Zhao, ACS Appl. Mater. Interfaces, 2017, **9**, 30832-30839.

5 L.-F. Chen, X.-D. Zhang, H.-W. Liang, M. Kong, Q.-F. Guan, P. Chen, Z.-Y. Wu and S.-H. Yu, ACS nano, 2012, **6**, 7092-7102.

6 A. M. Khattak, H. Sin, Z. A. Ghazi, X. He, B. Liang, N. A. Khan, H. R. Alanagh, A. Iqbal, L. Li and Z. Tang, J. Mater. Chem. A, 2018, **6**, 18827-18832.

7 S. Y. Park, C. W. Kang, S. M. Lee, H. J. Kim, Y.-J. Ko, J. Choi and S. U. Son, Chem. Eur. J, 2020, **26**, 12343-12348.

8 L. Mei, X. Cui, Q. Duan, Y. Li, X. Lv and H.-G. Wang, Int. J. Hydrog. Energy, 2020, **45**, 22950-22958.

9 C. R. Deblase, K. Hernández-Burgos, K. E. Silberstein, G. G. Rodríguez-Calero, R. P. Bisbey, H. D. Abruña and W. R. Dichtel, ACS nano, 2015, **9**, 3178-3183.

10 R. Xue, H. Guo, L. Yue, T. Wang, M. Wang, Q. Li, H. Liu and W. Yang, New J. Chem., 2018, **42**, 13726-13731.

11 A. M. Khattak, Z. A. Ghazi, B. Liang, N. A. Khan, A. Iqbal, L. Li and Z. Tang, J. Mater. Chem. A, 2016, **4**, 16312-16317.

12 M. G. Mohamed, X. Zhang, T. H. Mansoure, A. F. M. El-Mahdy, C.-F. Huang, M. Danko, Z. Xin and S.-W. Kuo, Polymer, 2020, **205**, 122857.

13 W. Yang, B. Huang, L. Li, K. Zhang, Y. Li, J. Huang, X. Tang, T. Hu, K. Yuan and Y. Chen, Small Methods, 2020, **4**, 2000434.

14 A. F. M. El-Mahdy, C.-H. Kuo, A. Alshehri, C. Young, Y. Yamauchi, J. Kim and S.-W. Kuo, J. Mater. Chem. A, 2018, **6**, 19532-19541.

15 C. R. Deblase, K. E. Silberstein, T.-T. Truong, H. D. Abruña and W. R. Dichtel, J. Am. Chem. Soc., 2013, **135**, 16821-16824.